



# Determination of Useful Life of Red Ceramic Parts Incorporated with Ornamental Stone Waste

Gustavo de Castro Xavier, Ph.D.<sup>1</sup>; Afonso Rangel Garcez de Azevedo, Ph.D.<sup>2</sup>; Jonas Alexandre, Ph.D.<sup>3</sup>; Sergio Neves Monteiro, Ph.D.<sup>4</sup>; and Leonardo Gonçalves Pedroti, Ph.D.<sup>5</sup>

**Abstract:** This study investigated, on a laboratory scale, the effect of the durability of the incorporation of ornamental stone waste in the production of red ceramic parts in order to improve material properties and durability. To reach this objective, ornamental stone waste material, of up to 10% by mass, was introduced to the red ceramic mass. Several other techniques were employed, including X-ray fluorescence chemical analysis, differential thermal analysis, and X-ray diffraction analysis. The samples, pressed to dimensions of  $11.0 \times 2.5 \times 1.0$  cm with 8% humidity, were oven dried and sintered at 750°C, 850°C, and 950°C and analyzed for water absorption, linear shrinkage, and flexural strength. To predict the strength behavior of the red ceramic parts over time (or over the long term), a low-cost experimental procedure was used to relate the accelerated degradation time in the laboratory for 200 days of saturation and oven-drying cycles at 110°C to the time exposure of the samples to weathering, in this case, for 5 years. The wetting–drying cycles were used to represent the most unfavorable environmental condition for deterioration processes, and the choice of flexural strength over the other properties was due the higher effect of degradation on this property. The useful life of red ceramic parts was defined as when the minimum value of 1.5 MPa was reached, obtaining 14 years for samples sintered at 950°C with stone waste content of 5% by mass and 4.8 years for samples sintered at 950°C with stone waste content of 0% by mass. The durability of red ceramic parts made with stone waste increased 2.91-fold due to the alkali and earth alkali of the stone waste that form molten flux during sintering and the vitreous phase during cooling, closing pores, and thus improving product quality. Furthermore, the stone waste material was inert, leading to proper disposal in the environment. DOI: [10.1061/\(ASCE\)MT.1943-5533.0002590](https://doi.org/10.1061/(ASCE)MT.1943-5533.0002590). © 2018 American Society of Civil Engineers.

**Author keywords:** Red ceramics; Ornamental stone waste; Durability; Useful life.

## Introduction

Industrial waste and its recycling have been of great interest and environmental importance in the industrial and scientific community since enormous quantities of such wastes are generated by various types of production processes in Brazil and in the rest of the world (Rozenstrauha et al. 2006; Monteiro and Vieira 2014; Mynim et al. 2017).

In recent years, the ceramic industry has played an important role in the recycling of these industrial wastes as an alternative raw material for the manufacture of ceramic products for civil

construction (Rozenstrauha et al. 2006; Acchar et al. 2006a, b; Xavier et al. 2012, 2014; Gomes et al. 2014; Ribeiro et al. 2015; Santos et al. 2015; Alexandre et al. 2016).

In this respect, the city of Campos dos Goytacazes, located in the northern region of the State of Rio de Janeiro, Brazil (Campos-RJ), has a large reserve of clays and approximately 100 red ceramic industries producing  $90 \times 10^6$  clay components/month, mostly ceramic bricks. In addition, the clay from this region has a predominance of kaolinite, a natural material that contributes to the high plasticity of clay (Vieira et al. 2004). As a consequence, ceramic parts have high porosity (Torres et al. 2009; Vieira et al. 2004, 2016) and dimensional defects. In addition, the high alumina concentration in this clay produces a refractory character in the material, making it difficult to sinter the pieces during firing (Vieira et al. 2016). These materials have some properties that may limit their use, such as low tensile strength relative to compressive strength, brittle rupture behavior, and high stress dispersion (Munz and Fett 1999).

The mineral and oxide composition of the raw materials and the texture of the sintered ceramic part, resulting from the physical and chemical changes provoked during firing, determine the durability, strength, and other characteristics of the pieces (Stryzewska 2014).

In an effort to improve the ceramic properties and increase the durability of the parts, a nonbiodegradable ornamental stone waste (Saboya et al. 2007) was used, with particles varying between 2 and  $60 \mu\text{m}$ , chemically similar to the clay of Campos-RJ.

The stone waste comes from the abrasion caused by the movement of the diamond wire saw in the process of cutting a block of rock, transforming it into plates. The estimated amount of waste from this process in the municipality of Cachoeiro de Itapemirim, Espírito Santo, Brazil (Itapemirim-ES), 150 km from

<sup>1</sup>Professor, Civil Engineering Laboratory, State Univ. of the Northern Rio de Janeiro, Av. Alberto Lamego, 2000, Campos dos Goytacazes, Rio de Janeiro 28013-602, Brazil. Email: gxavier@uenf.br

<sup>2</sup>Professor, Civil Engineering Laboratory, State Univ. of the Northern Rio de Janeiro, Av. Alberto Lamego, 2000, Campos dos Goytacazes, Rio de Janeiro 28013-602, Brazil (corresponding author). Email: afonso.garcez91@gmail.com

<sup>3</sup>Professor, Civil Engineering Laboratory, State Univ. of the Northern Rio de Janeiro, Av. Alberto Lamego, 2000, Campos dos Goytacazes, Rio de Janeiro 28013-602, Brazil. Email: jonas@uenf.br

<sup>4</sup>Professor, Engineering and Materials Science, Military Engineering Institute, Praça Gen. Tibúrcio, No. 80, Urca, Rio de Janeiro, Rio de Janeiro 28013-602, Brazil. Email: snevesmonteiro@gmail.com

<sup>5</sup>Professor, Dept. of Civil Engineering, Federal Univ. of Viçosa, Av. P.H. Rolfs, Viçosa, Minas Gerais 36570-000, Brazil. Email: lpedroti@gmail.com

Note. This manuscript was submitted on February 5, 2018; approved on August 2, 2018; published online on November 30, 2018. Discussion period open until April 30, 2019; separate discussions must be submitted for individual papers. This paper is part of the *Journal of Materials in Civil Engineering*, © ASCE, ISSN 0899-1561.

Campos-RJ, Brazil's largest ornamental rock producer, is approximately 150 thousand tons/month (Rodrigues et al. 2012).

This stone waste, in the form of slurry, is disposed of in landfills and settling ponds, which can cause environmental damage by contamination of surface water, groundwater, soils, rivers, and lakes.

The objective of this study is to determine the durability of ceramic parts that have incorporated ornamental stone waste. The degradation time in the laboratory (200 cycles of wetting and drying) is correlated with the natural degradation time from exposure to local weathering (5 years), until the ceramic parts weaken and reach the minimum flexural strength value of 1.5 MPa for ceramic bricks (Santos 1989). Scanning electron microscopy (SEM) was used to evaluate the properties of the red ceramic parts, and the environmental class of the stone waste was also determined.

## Materials and Methods

### Materials

The raw materials used in this investigation were clay from Campos-RJ and ornamental stone waste from Itapemirim-ES [Figs. 1(a and b)].

### Methods

The objective of the experimental program was to identify and obtain the technological properties of the materials used, as well as the useful life of the product, i.e., the time in which the flexural strength of the ceramic samples incorporated with ornamental stone waste reach the minimum value, as compared with ceramic parts without the waste material. In addition, the molten flux attributable to the incorporated waste material was investigated in terms of the probability of rupture, the mechanical behavior, and the aging of the material.

### Characterization

Particle size analysis of the clay and the ornamental stone waste was determined according to NBR 7181 (ABNT 1984). Then the mineralogical, chemical, and thermal analyses of the clay and the stone waste were carried out. First, the samples were passed through a No. 200 mesh (0.074 mm) sieve and placed in an oven at 110°C. The qualitative mineralogical composition was obtained by X-ray diffractometry using Shimadzu XRD-7000 equipment

(São Paulo, Brazil). The generator settings were 30 kV and 30 mA, Cu-K $\alpha$ 1 radiation, angular step of 0.02°, time interval of 1 s, and 2 $\theta$  varying from 5° to 60°. The minerals present in the clay and waste material were identified in reference to the International Centre for Diffraction Data (ICDD) PDF-2 database. The powder diffraction file (PDF) cards are 01-078-1996 kaolinite, 00-046-1045 quartz, 01-086-1384 Muscovite, 01-075-5065 goethite, 00-021-1272 anatase, 00-010-0393 albite, 01-071-1540 orthoclase, 01-076-6571 biotite, and 01-080-2791 calcite. The quantification of crystalline phases was obtained with Shimadzu XRD-6100/7000 software (version 7.0), under the same conditions. The parameters refinement included background, weight fractions, lattice parameters, and specimen displacement correction. To model the profile from peaks (including width) the Scherrer equation and the intermediate Lorentzian and pseudo-Voigt functions were used. The energy-dispersive X-ray equipment, Shimadzu Model EDX700, was used for chemical analysis. The loss-on-ignition (LOI) test was conducted in an electronic muffle oven at 1,000°C. Differential thermal analysis was performed using 30 mg of each sample in a nitrogen atmosphere at a rate of 10°C/min up to 1,020°C in universal testing equipment, Model V2.6D from TA Instruments (New Castle, Delaware). The leaching and solubilization test followed the procedures of NBR 10005 (ABNT 2004a) and NBR 10006 (ABNT 2004b). The following equipment was used: a turbidimeter (Micronal Model B250, São Paulo, Brazil) for sulfate identification, a spectrophotometer (Shimadzu UVmini-1240) for chloride, flame photometer (Micronal Model B261) for sodium, an atomic absorption spectrophotometer (Perkin Elmer AAnalyst 300, São Paulo, Brazil) for Cr, Pb, Cu, and Mn, and an inductively coupled plasma atomic emission spectrometer (Perkin Elmer) for Ag, As, Al, Ba, Fe, Zn, and Cd. The maximum permissible concentrations were classified according to NBR 10004 (ABNT 2004c).

### Preparation of Samples

Samples dried at 110°C were sieved in a No. 20 mesh sieve (0.84 mm opening), incorporated with stone waste content of 0% (0W), 5% (5W), and 10% (10W) by mass (Table 1) and then passed through a ball mill for homogenization. The material was then hydrated to an 8% moisture content.

The ceramic parts were pressed at 25 MPa in prisms of 11.0 × 2.5 × 1.0 cm. The mean represents 13 samples ( $N$ ). Then the ceramic parts were oven dried 110°C and sintered at 750°C, 850°C, and 950°C in an electronic muffle oven with a firing rate of 2°C/min and a baseline firing time of 3 h. Cooling occurred

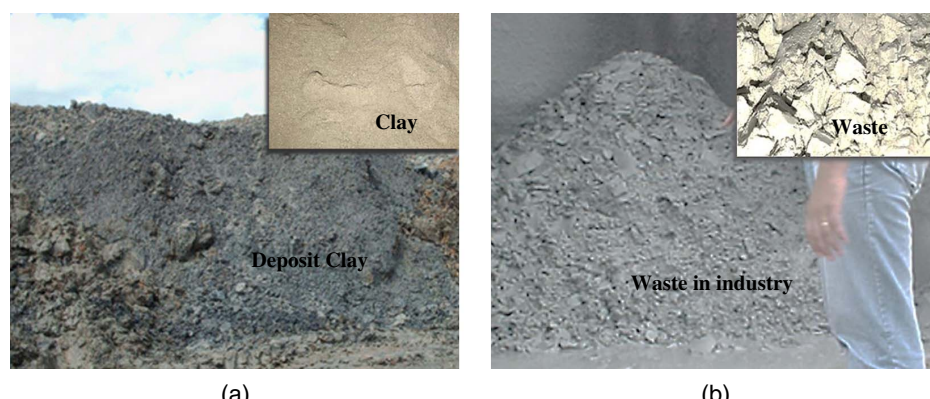


**Fig. 1.** (a) Clay; and (b) ornamental stone waste.

**Table 1.** Clay sample composition

Sample	Composition (%)	
	Clay	Waste
0W	100	0
5W	95	5
10W	90	10

overnight at room temperature. This lot will henceforth be referred to as intact samples (versus degraded samples).

### Technological Properties

For each clay–stone residue composition (mixture), 13 samples were tested to obtain water absorption (ASTM 1972), apparent porosity (ASTM 1972), linear shrinkage (Santos 1989), and flexural strength using the three-point method (ASTM 1977). The loading rate was 0.5 mm/min and the distance between the supports was 9 cm. Table 2 presents the dimensions and the values for the sample properties (mean  $\pm$  standard deviation).

The Weibull distribution was used to determine the probability of failure caused by internal defects in the intact parts and to analyze the modulus  $m$ . The Weibull statistic describes the probability of failure of the material when subjected to a certain stress (Somiya 1990). The probability of survival or failure was calculated using the cumulative distribution function for symmetric samples (Murthy et al. 2004), using the most accurate probability estimator  $P$  [Eq. (1)]

$$P = \frac{(i - 0.3)}{(N + 4)} \quad (1)$$

where  $i$  = index of ascending order of failure; and  $N$  = number of samples. The characteristic stress was determined for the 63.2% probability below which the material did not fail.

To obtain the stress-strain curve, Strain Gauge PA-06-1000BA-120L was used, connected to a Lynx-type data acquisition system, and interpreted by AqDados and AqDAnalysis software. The modulus of elasticity  $E$  in the three-point bending flexural test was calculated by Eq. (2)

$$E = \frac{PL^3}{48I\nu} \quad (2)$$

**Table 2.** Samples' dimensions and technological properties when intact

Sample	Temperature (°C)	L $\pm$ SD (cm)	w $\pm$ SD (cm)	H $\pm$ SD (cm)	LS $\pm$ SD (%)	WA $\pm$ SD (%)	FS $\pm$ SD (MPa)
0W	Moisture (8%) at 21°C	11.53 $\pm$ 0.02	2.54 $\pm$ 0.01	1.05 $\pm$ 0.03	—	—	—
	750	11.41 $\pm$ 0.03	2.54 $\pm$ 0.01	1.05 $\pm$ 0.03	1.01 $\pm$ 0.31	22.5 $\pm$ 0.40	2.60 $\pm$ 0.20
	850	11.40 $\pm$ 0.02	2.53 $\pm$ 0.01	1.05 $\pm$ 0.03	1.24 $\pm$ 0.31	22.0 $\pm$ 0.60	3.00 $\pm$ 0.30
	950	11.29 $\pm$ 0.02	2.51 $\pm$ 0.01	1.01 $\pm$ 0.02	1.88 $\pm$ 0.21	21.0 $\pm$ 0.30	4.20 $\pm$ 0.20
5W	Moisture (8%) at 21°C	11.53 $\pm$ 0.01	2.54 $\pm$ 0.01	1.05 $\pm$ 0.04	—	—	—
	750	11.42 $\pm$ 0.03	2.53 $\pm$ 0.01	1.04 $\pm$ 0.04	0.90 $\pm$ 0.26	21.50 $\pm$ 0.40	2.90 $\pm$ 0.20
	850	11.41 $\pm$ 0.04	2.53 $\pm$ 0.01	1.04 $\pm$ 0.03	0.88 $\pm$ 0.26	20.50 $\pm$ 0.20	3.40 $\pm$ 0.20
	950	11.30 $\pm$ 0.02	2.51 $\pm$ 0.01	1.04 $\pm$ 0.03	1.90 $\pm$ 0.29	20.00 $\pm$ 0.20	4.60 $\pm$ 0.20
10W	Moisture (8%) at 21°C	11.52 $\pm$ 0.02	2.54 $\pm$ 0.01	1.05 $\pm$ 0.01	—	—	—
	750	11.44 $\pm$ 0.02	2.54 $\pm$ 0.01	1.05 $\pm$ 0.01	0.65 $\pm$ 0.19	21.90 $\pm$ 0.30	2.60 $\pm$ 0.20
	850	11.42 $\pm$ 0.01	2.53 $\pm$ 0.01	1.05 $\pm$ 0.01	0.81 $\pm$ 0.22	21.00 $\pm$ 0.40	3.00 $\pm$ 0.20
	950	11.38 $\pm$ 0.02	2.52 $\pm$ 0.01	1.05 $\pm$ 0.01	1.43 $\pm$ 0.25	20.50 $\pm$ 0.30	4.30 $\pm$ 0.15

Note: Samples tested in February 2012. L = length; SD = standard deviation; w = width; H = height; LS = linear shrinkage; WA = water absorption; and FS = flexural strength.

where  $P$  = charge (N);  $L$  = distance between cuts (mm);  $I$  = moment of inertia ( $\text{mm}^4$ ); and  $\nu$  = deflection (vertical displacement of sample) (mm).

### Durability Tests

Motivated by the scarcity of results for the long-term durability of red ceramic parts, this study investigated deterioration due to (or caused by) climatic conditions. The majority of durability problems with red ceramic parts in the Campos-RJ region were linked to the use of low sintering temperatures, which allow for the transport of moisture through the pores to the interior of the part when exposed to the wetting–drying cycles of the environment, especially in tropical climates.

The wetting–drying cycles have been identified as the most unfavorable environmental condition in the deterioration processes (Brooks and Cetin 2013). The accelerated degradation mechanisms considered in wetting–drying cycles considered in this study were the temperature variation from day (sun) to night, and the rainfall and relative humidity.

Given these considerations, a batch of the ceramic material was subjected to the laboratory degradation process by means of saturation and drying cycles, immersing the red ceramic parts in water for 10 h and placing them in an oven at 110°C for 14 h, according to Xavier et al. (2012). Up to 200 cycles were performed. The 5-year weathering of the other batch of the ceramic material occurred on the roof of one of the State University of Northern Rio de Janeiro (UENF) buildings with a slope equal to 21°48' relative to horizontal, corresponding to latitude 21°48'14" S and longitude 41°19'26" W, to ensure a higher incidence of solar radiation. The climatic characteristics of the weathering region include temperatures ranging from 20°C to 31°C, 270 days of annual precipitation with a cumulative value of 3,165 mm, and relative humidity of 79%. The highest solar irradiance rate per month was 700 MJ/m<sup>2</sup> and 18 GJ/m<sup>2</sup> for total solar energy irradiation (INMET 2016).

After cycling and weathering (Fig. 2), the following technological properties were determined: water absorption, apparent porosity, linear shrinkage, flexural strength, modulus  $m$ , and the stress-strain curve of the material. Table 3 presents the dimensions and the results of the properties of the samples (mean  $\pm$  standard deviation). The dimensions were obtained using a Mitutoyo (São Paulo, Brazil) paquimeter (precision  $\pm$  0.01 mm). Fig. 2 shows the degraded edges and discolored surface.

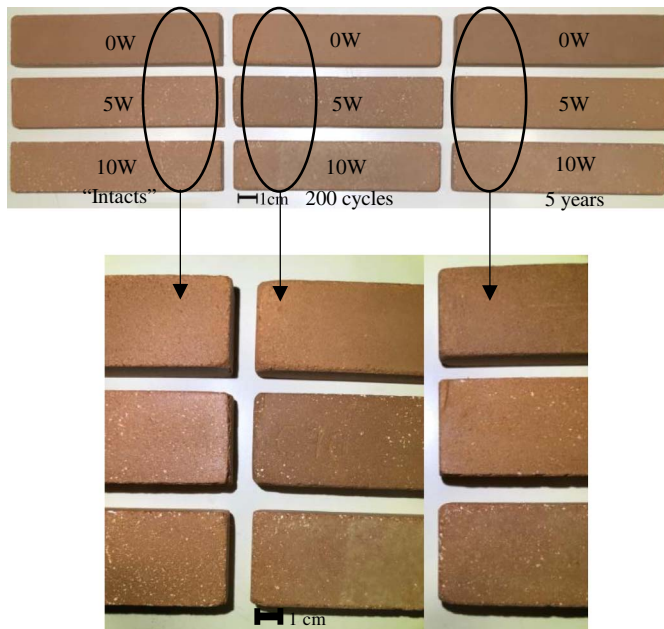


**Fig. 2.** Samples before and after 200 cycles and 5 years of weathering. All samples were sintered at 950°C.

To define durability, the loss of flexural strength index  $I_{LFS}$  was calculated in each degradation process using Eq. (3)

$$I_{LFS} = \frac{|FS_0 - FS|}{FS_0} \times 100\% \quad (3)$$

The  $I_{LFS}$  relates the parameter of the intact sample,  $FS_0$ , to the parameter of the degraded sample,  $FS$ . The value of the loss of flexural strength index varies from zero for the intact material to a maximum value, always less than 100%, for the most degraded material. Based on the obtained values (Tables 2 and 3), the  $I_{LFS}$  (%) was calculated for each set of samples after the degradation times, thereby relating the laboratory degradation time, 200 cycles, with the weatherization period of up to 5 years, provided it has the same loss of flexural strength index value [Fig. 13(a)]. Given the correlation of times obtained directly from the  $I_{LFS}$  curves, the equations can be found to define the time in which the material will lose strength, up to the minimum allowed, that is, its durability [Fig. 13(b)]. To clarify, Fig. 13(a) shows degradation times after 200 cycles (175 days) and for 1,825 days (5 years) for

the same  $I_{LFS}$  (56%), yielding a point on the adjusted curve of Fig. 13(b).

The surface morphology of the samples before and after degradation was analyzed with a scanning electron microscope (Shimadzu SSX-550) operating at 15 kV.

## Results and Discussion

### Characteristics of Raw Materials

Fig. 3 shows the particle size distribution of the clay and stone waste material.

Fig. 3 shows a broad particle size range for the studied clay, between 1.2 and 100  $\mu\text{m}$ . The percentage of clay particles  $<2 \mu\text{m}$  was 48.8%, which is considered high and responsible for the plasticity during molding and strength after heat treatment (Vieira et al. 2004, 2016). The proportion of clay particles between 2 and 60  $\mu\text{m}$  was 48.5% and that of sand particles ( $>60 \mu\text{m}$ ) was 2.6%, characterizing it as a typical plastic clay for ceramic use.

The particle size distribution of the 87% of ornamental stone waste between 2 and 60  $\mu\text{m}$  is considered to be fine material, and promotes better packing when incorporated into the clay. The proportion of particles smaller than 2  $\mu\text{m}$ , fine particles of mica, was 10.9% (Fig. 4), and the percentage of particle size classified as sand, or coarse particles of the waste, was less than 2%. These results are similar to those reported by Vieira et al. (2016). The stone waste material was classified as nonplastic.

Fig. 4 shows the X-ray diffractograms of the clay [Fig. 4(a)] and the stone waste [Fig. 4(b)].

The X-ray diffractogram shows the presence of kaolinite (63.3%), quartz (12.7%), muscovite (12.0%), goethite (10.5%), and anatase (1.20%). The results in Fig. 1 with a particle size of up to 60  $\mu\text{m}$  add up to more than 97% and the sum of the clay and minerals present is 87%, disregarding the quartz. On the other hand, fine particles of quartz up to 60  $\mu\text{m}$  can be found, so the results in Figs. 3 and 4 and Table 4 converge.

The X-ray diffractogram of the stone waste [Fig. 4(b)] shows the presence of albite (47.8%) quartz (20%), orthoclase (14.7%), muscovite (13.2%), biotite (2.3%), and calcite (2.1%). These particles are predominantly in the fraction up to 60  $\mu\text{m}$  (Fig. 3) and may contribute to the formation of molten flux during sintering, facilitating vitreous formation during cooling (Acchar et al. 2006b).

The chemical compositions of clay and stone waste are shown in Table 5.

The composition of  $\text{SiO}_2 + \text{Al}_2\text{O}_3$  above 84% characterizes the clay mass as refractory. The amount of aluminum oxide  $\text{Al}_2\text{O}_3$  (35.6%) indicates a high presence of kaolinite, as shown in Fig. 4

**Table 3.** Samples' dimensions and technological properties after 200 cycles

Sample	Temperature (°C)	L $\pm$ SD (cm)	w $\pm$ SD (cm)	H $\pm$ SD (cm)	LS $\pm$ SD (%)	WA $\pm$ SD (%)	FS $\pm$ SD (MPa)
0W	750	11.40 $\pm$ 0.02	2.53 $\pm$ 0.01	1.02 $\pm$ 0.01	1.04 $\pm$ 0.11	23.90 $\pm$ 0.55	1.00 $\pm$ 0.20
	850	11.38 $\pm$ 0.02	2.53 $\pm$ 0.01	1.01 $\pm$ 0.04	1.12 $\pm$ 0.17	23.31 $\pm$ 0.40	1.60 $\pm$ 0.20
	950	11.29 $\pm$ 0.01	2.50 $\pm$ 0.02	1.00 $\pm$ 0.01	1.97 $\pm$ 0.20	22.00 $\pm$ 0.50	1.70 $\pm$ 0.15
5W	750	11.39 $\pm$ 0.01	2.53 $\pm$ 0.01	1.01 $\pm$ 0.02	1.08 $\pm$ 0.30	23.50 $\pm$ 0.30	1.30 $\pm$ 0.20
	850	11.36 $\pm$ 0.01	2.53 $\pm$ 0.01	1.01 $\pm$ 0.02	1.37 $\pm$ 0.20	23.00 $\pm$ 0.30	1.80 $\pm$ 0.30
	950	11.30 $\pm$ 0.01	2.51 $\pm$ 0.01	1.01 $\pm$ 0.03	2.03 $\pm$ 0.03	20.50 $\pm$ 0.50	2.70 $\pm$ 0.15
10W	750	11.37 $\pm$ 0.02	2.53 $\pm$ 0.01	1.00 $\pm$ 0.03	0.86 $\pm$ 0.30	23.40 $\pm$ 0.53	1.10 $\pm$ 0.20
	850	11.35 $\pm$ 0.02	2.52 $\pm$ 0.01	1.00 $\pm$ 0.02	1.05 $\pm$ 0.20	23.50 $\pm$ 0.30	1.60 $\pm$ 0.20
	950	11.24 $\pm$ 0.03	2.50 $\pm$ 0.01	1.00 $\pm$ 0.04	1.75 $\pm$ 0.15	21.50 $\pm$ 0.40	2.00 $\pm$ 0.15

Note: Samples tested in January 2014. L = length; SD = standard deviation; w = width; H = height; LS = linear shrinkage; WA = water absorption; and FS = flexural strength.

and Table 4. The red color of the clay after sintering is due to ferric oxide  $\text{Fe}_2\text{O}_3$  (8.87%) and titanium dioxide  $\text{TiO}_2$  (1.62%), in this case, present in the goethite and anatase, respectively (Fig. 4 and Table 4). In addition, potassium oxide  $\text{K}_2\text{O}$  (3.17%) in the clay forms a liquid phase at sintering above 700°C (Emiliani and Corbara 1999), penetrating the pores, reducing water absorption (Barba et al. 2002; Celik 2010; Ribeiro et al. 2015; Vieira and Emiliano 2015; Vieira et al. 2016). The remaining compounds below 1% do not interfere with the final product. The loss on ignition of the clay was 14.89%, considered high, indicating an elevated fraction of dehydroxylated clay minerals associated with the organic matter burn-off (Pérez-Villarejo et al. 2012), which lose mass at 1,000°C.

In the stone waste material, the silica content is above 55% and that of  $\text{Al}_2\text{O}_3$  is higher than 19%, indicating chemical compositions of primary minerals (Table 2). The  $\text{Fe}_2\text{O}_3$  content (12.47%) contributes to the red color of the part and is contained in the biotite (Table 2). The  $\text{K}_2\text{O} + \text{Na}_2\text{O}$  (6.75%) is associated with the albite and the orthoclase of the stone waste (Table 4) and is important during sintering for the reduction of pores. The  $\text{CaO}$  (2.99%) is associated with calcium carbonate ( $\text{CaCO}_3$ ), which is mineral cement and similar to the results found in Table 4. The loss on ignition of the stone waste material is low (1.86%), showing

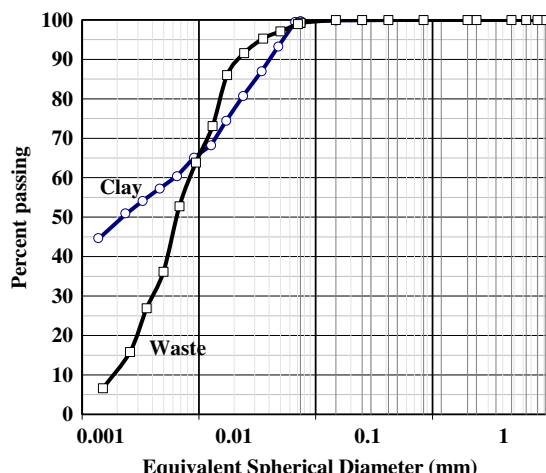


**Fig. 3.** Particle size distribution of the raw materials.

stability in temperatures used. The thermogram [differential thermal analysis (DTA) and thermogravimetry (TG)] of the clay is shown in Fig. 5.

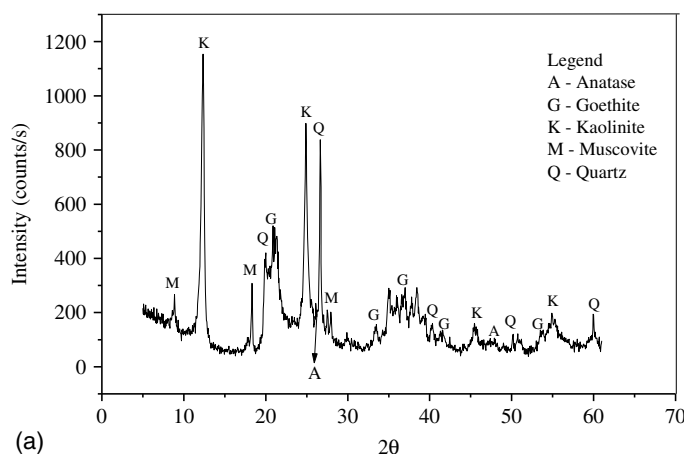
Fig. 5 shows two endothermic peaks related to a mass loss of 15.6% for the clay investigated. This value is close to the loss on ignition (14.89%) shown in Table 5. The first endothermic event, at 260.9°C, is related to dehydroxylation of goethite  $[\text{Al}(\text{OH})_3]$  and the second event, at 499.5°C, is the dehydroxylation of kaolinite, transforming into metakaolinite (Saboya et al. 2007; Vitorino et al. 2009). These results agree with the predominance of kaolinite among the other crystalline phases found in Fig. 4 and Table 4.

Fig. 6 shows two endothermic peaks related to a loss of mass of 2.1% for the stone waste material, similar to the loss on ignition (1.86%) given in Table 5. The first event, at 570°C, corresponds to allotropic transformation of quartz  $\alpha$  to  $\beta$  (Nandi et al. 2015), with a slight expansion; and the second event, at 663.18°C, is due to the degradation of the micas present [muscovite + biotite = 15.5% (Table 4)] (Saboya et al. 2007).

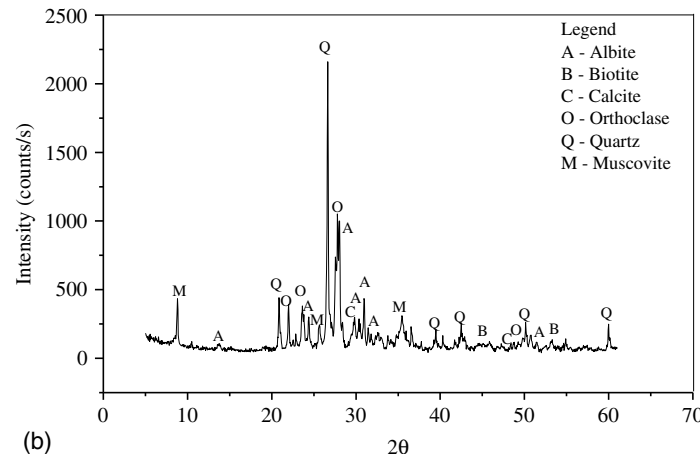
The environmental analysis of the sample of ornamental stone waste, for the 0W clay and the 5W clay is presented in Tables 6 and 7 for the leaching [NBR 10005 (ABNT 2004a)] and solubilization tests [NBR 10006 (ABNT 2004b)]. The results of leaching of the inorganic extract from the stone waste material (Table 6), the clay, and the 5W clay show the presence of heavy metals Ag, As,

**Table 4.** Quantification of minerals by Rietveld method of the raw materials

Crystalline phase	Percentage
Clay	
Kaolinite	63.3
Quartz	12.7
Muscovite	12.0
Goethite	10.5
Anatase	1.2
Waste	
Albite	47.8
Quartz	20.0
Orthoclase	14.7
Muscovite	13.2
Biotite	2.3

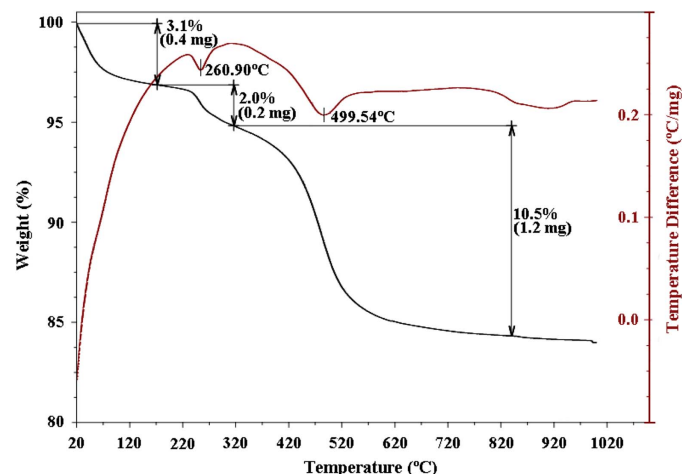
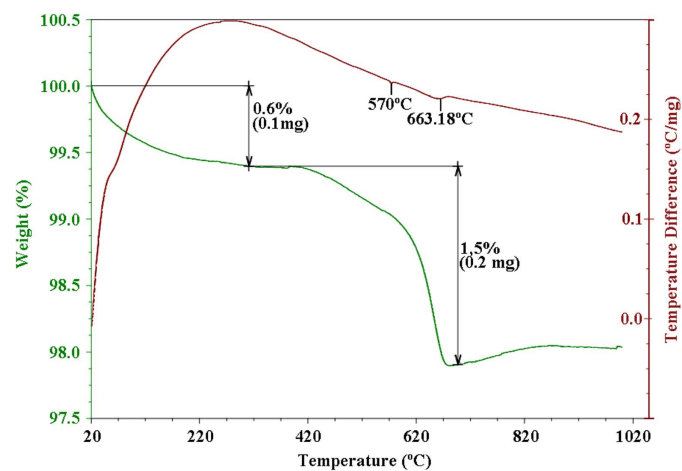


**Fig. 4.** X-ray diffraction patterns of the raw materials.



**Table 5.** Chemical composition of the raw materials

Raw materials	SiO <sub>2</sub> (%)	Al <sub>2</sub> O <sub>3</sub> (%)	Fe <sub>2</sub> O <sub>3</sub> (%)	K <sub>2</sub> O (%)	Na <sub>2</sub> O (%)	TiO <sub>2</sub> (%)	SO <sub>3</sub> (%)	CaO (%)	MnO (%)	LOI (%)
Clay	48.83	35.46	8.87	3.17	—	1.62	0.90	0.89	0.26	14.89
Waste	55.09	19.86	12.47	3.70	3.05	1.83	—	2.99	1.00	1.86

**Fig. 5.** Thermogram (DTA/TG) of the clay.**Fig. 6.** Thermogram (DTA/TG) of ornamental stone waste.

Cd, Cr, Pb, and Ba in concentrations below the maximum limits established in Annex F of NBR 10004 (ABNT 2004c). Therefore, in the present study, the waste can be considered nonhazardous and nontoxic (Manhães and Holanda 2008; Nandi et al. 2015).

Table 7 presents the results of the solubilization test. With the exception of Fe, the results show that the stone residue, the 0W clay, and the 5W clay did not exceed the limits established by Annex G of NBR 10004 (ABNT 2004c). The slightly higher concentrations of Fe classify the residue material, the 0W clay, and the 5W clay as class IIA residue—not inert and nonhazardous. This elevated concentration of Fe is associated with the biotite and goethite shown in Fig. 4 and Table 4, oxidizing during sintering, giving the ceramics a red color. In the case of disposal of this material, because of defects or after demolition, it is not hazardous (Vieira et al. 2016).

**Table 6.** Inorganic leaching test results of waste, 0W clay, and 5W clay

Chemical element	Waste (mg/L)	0W clay (mg/L)	5W clay (mg/L)	Uncertainties (±)	Leached maximum limit <sup>a</sup> (mg/L)
Ag	<0.004	<0.002	<0.015	0.00046	5.000
As	<0.010	<0.010	<0.010	0.00034	0.010
Cd	<0.001	<0.002	<0.055	0.000044	0.500
Cr	0.010	<0.009	<0.010	0.00097	5.000
Pb	0.020	<0.005	<0.002	0.00051	5.000
Ba	0.150	1.130	0.450	0.035	100.000
pH initial	9.100	10.300	9.100	1.00	NS
pH final	4.950	6.500	5.000	1.00	NS
Acid volume (mL)	80	130	400	0.0016	NS
Time (h)	28	28	28	—	NS

Note: NS = not specified.

<sup>a</sup>Brazilian Association of Technical Standards (ABNT 2004c)—attached F.

**Table 7.** Solubilization test results of waste, 0W clay, and 5W clay

Chemical element	Waste (mg/L)	0W clay (mg/L)	5W clay (mg/L)	Uncertainties (±)	Solubilized maximum limit <sup>a</sup> (mg/L)
Ag	<0.005	<0.001	0.070	0.000460	0.050
As	<0.010	<0.010	<0.010	0.000340	0.010
Cd	<0.002	<0.001	<0.001	0.000044	0.005
Cr	<0.030	<0.008	<0.010	0.000970	0.050
Pb	<0.060	<0.001	0.0410	0.00051	0.050
Ba	<0.020	0.020	0.030	0.035	1.000
Al	0.150	0.080	0.170	0.06	0.200
Cu	<0.010	<0.010	<0.040	0.00035	1.000
Fe	0.430	0.400	0.4000	0.0038	0.300
Mn	<0.010	<0.010	<0.010	0.0003	0.100
Zn	<0.020	<0.010	0.005	0.0038	5.000
Na	23.500	34.000	24.000	0.028	200.00
Chloride	9.440	8.000	10.500	0.022	250.00
Hardness (mg CaCO <sub>3</sub> /L)	19.900	19.700	19.990	0.75	500.00
Sulfate	11.170	<10.000	14.000	0.74	400.00

<sup>a</sup>Brazilian Association of Technical Standards (ABNT 2004a)—attached G.

### Technological Properties and Durability Tests

The physicomechanical properties are shown in Figs. 7–9 for samples 0W, 5W, and 10W after sintering, before and after degradation from the 200 wetting–drying cycles.

### Water Absorption of Intact Samples

Fig. 7(a) shows that water absorption in the intact samples varies little as a function of the same sintering temperature, regardless of the amount of stone waste incorporated. The exception was with the 5W clay at 950°C, which reaches the maximum limit of 20% in the case of ceramic tiles, the most refined product in the Campos-RJ

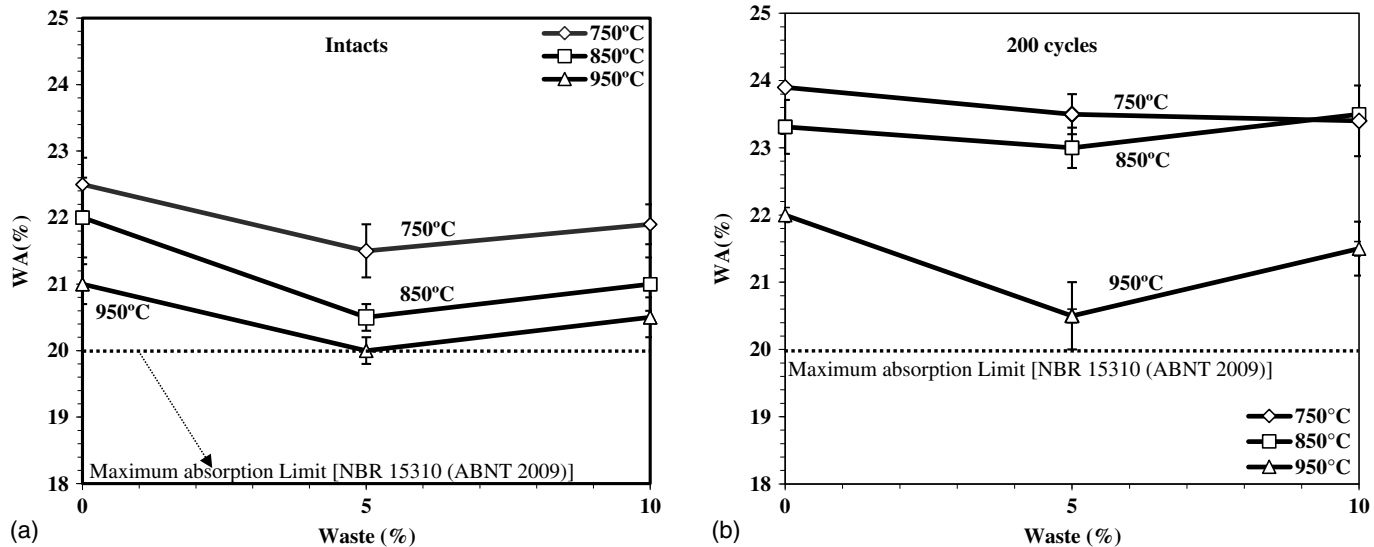


**Fig. 7.** Water absorption of the 0W, 5W, and 10W samples as a function the waste and sintering temperature: (a) before; and (b) after the degradation process.

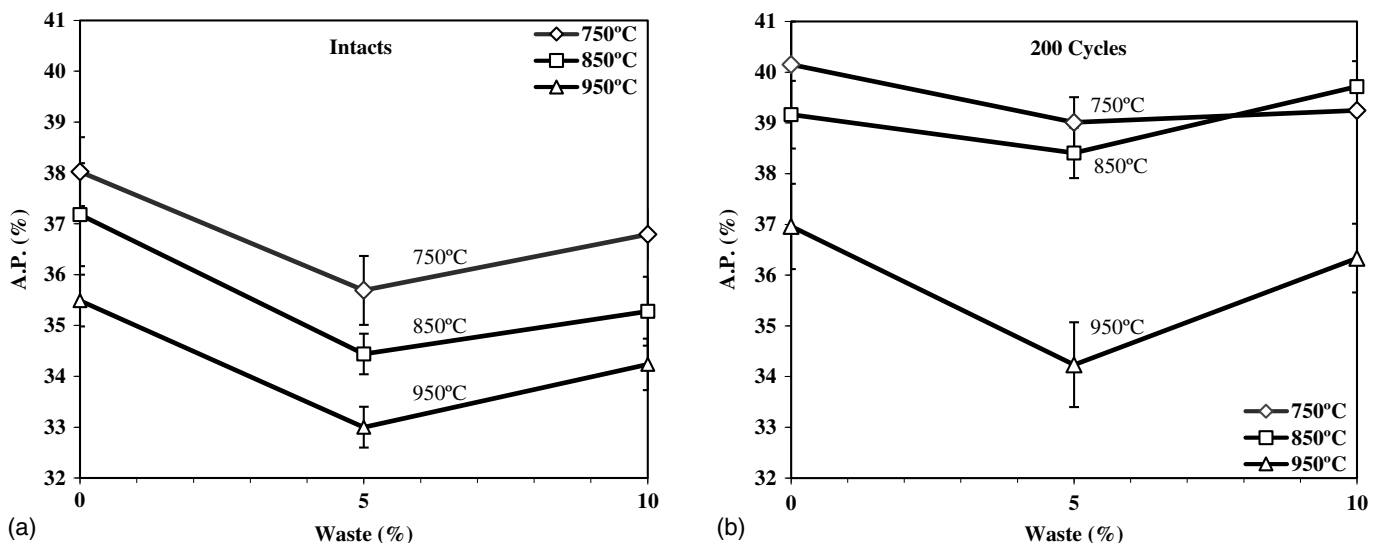


**Fig. 8.** Apparent porosity of the 0W, 5W, and 10W samples as a function the waste and sintering temperature: (a) before; and (b) after the degradation process.

region. There was an observed reduction in water absorption with the incorporation of the stone waste material in all cases, when compared with the sample with no stone waste (0W). This can be explained by the relatively high quantity of oxide flux in the waste material ( $K_2O + Na_2O + CaO > 9\%$ ) that forms a liquid phase and a partial dissolution of the quartz during sintering, filling the pores and forming a vitreous phase during cooling, as well as the low quantity of  $Al_2O_3$  shown in Table 5 (Vieira et al. 2016). There is no statistical difference between the 5W and 10W samples at the same sintering temperature since the standard deviations are coincident.

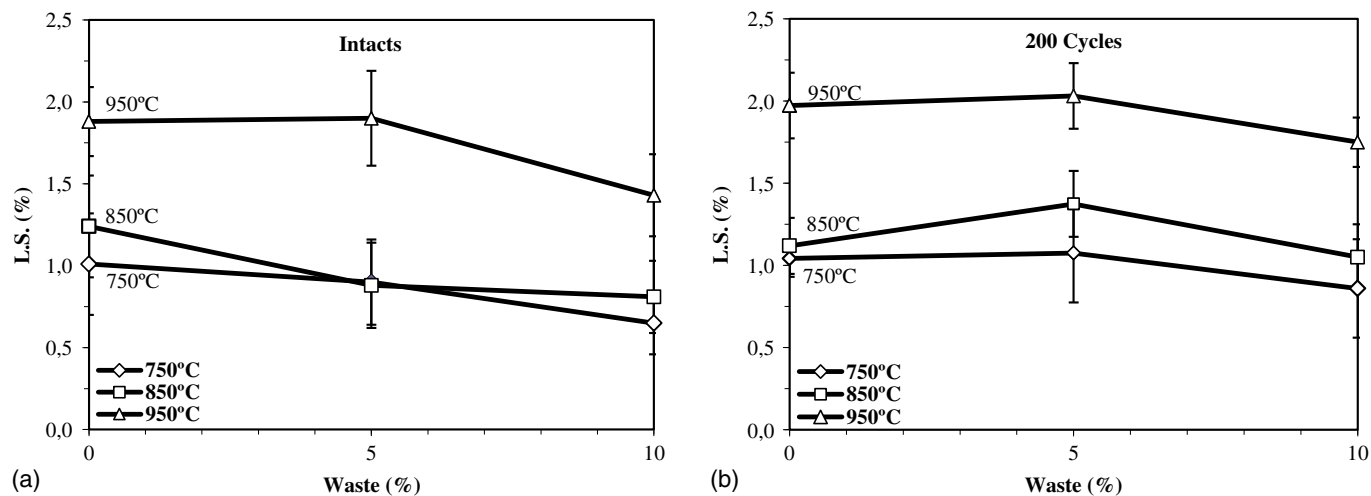
#### Water Absorption of Samples after 200 Cycles

Fig. 7(b) shows that the accelerated laboratory process of 200 wetting-drying cycles modified the water uptake of the samples, increasing in all cases. At both 750°C and 850°C, the 0W, 5W,

and 10W samples showed water absorption increases between 1.5% and 3%. The highest value was 24% for the 0W samples at 750°C. The 5W samples sintered at 950°C had smaller increments, remaining at the lower limit of the standard deviation, still at 20%. This porous (Fig. 8) and rough surface is recommended for the manufacture of bricks and red ceramic structural blocks, facilitating the adhesion of the mortar and plaster when used in civil construction projects. These results show that the incorporation stone waste material can contribute to ceramic processing, and increase durability since the furnaces of the Campos-RJ region do not reach 1,000°C. In addition, this application promotes a suitable disposition of the stone waste material.

#### Apparent Porosity of Intact Samples

It is noted in Fig. 8(a) that the 0W samples have higher apparent porosity values at all sintering temperatures. Furthermore,



**Fig. 9.** Linear shrinkage of the 0W, 5W, and 10W samples as a function of the waste and sintering temperature: (a) before; and (b) after the degradation process.

a decrease in the apparent porosity of the 5W samples at 950°C relative to the 0W and 10W samples is evident, with the results converging in Fig. 7(a). This is due to the alkali and earth alkali in the stone waste material (Table 5) that form molten flux during sintering and a vitreous phase during cooling, closing the pores (Vieira et al. 2004, 2016; Pérez-Villarejo et al. 2012). For the other temperatures and waste content levels, there was no statistical difference due to coincidence of the error bars.

#### Apparent Porosity of Samples after 200 Cycles

Fig. 8(b) shows the increase in the apparent porosity of the samples at all sintering temperatures and waste content levels, with the exception of the 5W samples at 950°C, in which there was an insignificant increase. In fact, the presence of alkali and earth alkali in the stone waste reduces the possibility of an increase of open pores by 5%, indicating increased durability relative to the other waste content levels.

#### Linear Shrinkage of Intact Samples

Fig. 9(a) shows the linear shrinkage of the intact 0W, 5W, and 10W samples at the indicated temperatures. The linear shrinkage on the order of 1% of the samples sintered up to 850°C did not present significant differences, that is, the stone waste at these temperatures did not interfere with the results. The samples at 950°C show linear shrinkage between 1.5% and 1.8%, being statistically the same, that is, independent of the incorporation of the stone waste. This shows that the stone waste does not modify the largest dimension of the red ceramic part at this sintering temperature. The higher linear retraction of the samples at 950°C is due to the sintering effects, forming a vitreous phase, mainly with the presence of K<sub>2</sub>O in the clay and K<sub>2</sub>O + Na<sub>2</sub>O + CaO in the stone waste (Table 5), joining the ceramic particles (Wiemes et al. 2017). In addition, the retraction is related to the loss of kaolinite hydroxylates (63.3%, Table 4, Fig. 5), increasing the sample packing. The linear retraction of the samples remained well below the limit of up to 8% for the production of ceramic bricks according to Okunade (2008).

#### Linear Shrinkage of Samples after 200 Cycles

In Fig. 9(b), the linear retraction of the samples after 200 wetting-drying cycles was not affected, that is, the samples remained stable

regardless of temperature or the level of stone waste incorporated. There was a tendency to increase the linear shrinkage in the samples at 950°C; however, this effect was not significant, and the error bars are coincident. The vitreous phase formation of the samples at the proposed temperatures was not affected for the linear retraction, remaining within the limit (of 8%) defined by Okunade (2008). For this property, these results are important for the manufacture of ceramic structural blocks, mainly in their application in architectural modulation. In practice, the modulation allows a variation of less than 5 mm [NBR 15270 (ABNT 2005)], so the results of linear shrinkage of ceramic pieces meet this requirement.

#### Flexural Strength of Intact Samples

All intact samples [Fig. 10(a)] had higher than the minimum value of flexural strength (of 1.5 MPa) defined by Santos (1989) for the manufacture of ceramic bricks. As the sintering temperature increases, strength increases, regardless of the level of stone waste incorporated. The 5W sample sintered at 950°C achieved the highest result of 4.6 MPa; however, at this temperature the deviations are coincident at all of the incorporation levels, that is, the flexural strength is independent of the addition of stone waste material of up to 10% by mass. This tendency for increase in strength is due to the lower water absorption [Fig. 7(a)], at the limit of 20%, smallest among all the intact samples. This is due to the low melting points of the oxides of the stone waste (K<sub>2</sub>O + Na<sub>2</sub>O + CaO; Table 5) after sintering at low temperatures, which contributes to the increase in strength. In this case, the clay particles have adhered and been fully encapsulated by the molten flux, forming vitreous structures (Myrmín et al. 2014; Wiemes et al. 2017).

The 0W samples yielded strength values ranging from 2.60 to 4.2 MPa, regardless of the sintering temperature, due to the low amount of oxide flux (Table 5) for the formation of viscous flow, open pores remaining without filling with glass (Vieira et al. 2004; Krakowiak et al. 2011; Pérez-Villarejo et al. 2012). This is also due to the dehydroxylation of kaolinite in greater quantity in the sample, making the sample more porous.

#### Flexural Strength of Samples after 200 Cycles

All samples in Fig. 10(b) present reduced flexural strength after 200 cycles of wetting and drying. The samples sintered at 750°C

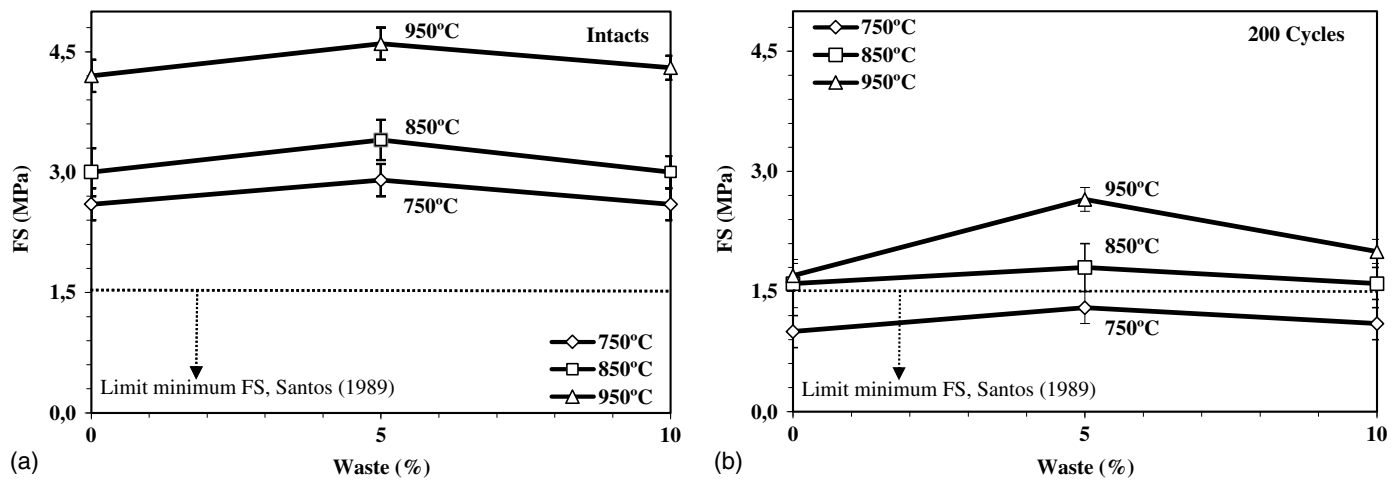


**Fig. 10.** Flexural strength of the 0W, 5W, and 10W samples as a function the waste and sintering temperature: (a) before; and (b) after the degradation process.

were below the minimum, that is, this temperature is not suitable for the manufacture of ceramic bricks for the proposed levels of incorporation of waste material. At 850°C, the values for the loss of flexural strength for all of the samples were significant, approaching the minimum.

The largest reduction in strength occurred with the 0W samples at 950°C after the cycles completed, reducing the initial strength (1.7 MPa) by 59.5%. This is due to the low amount of alkali in the sample for the formation of glass to fill the pores; consequently, the pores remain open [Fig. 8(b)], facilitating the flow of water to the interior of the part during saturation, allowing for cracking and an increase in defects. During the oven-drying process, the water that has penetrated the defects of the part vaporizes and is released, mobilizing the surface particles in contact with the water and steam in the ceramic part, causing more cracks.

The lowest reduction in strength, of 42.4% (2.7 MPa), occurred for the 5W samples sintered at 950°C. At this temperature, the presence of alkali and earth alkali form a vitreous structure in the pores and bring the clay particles closer, making it harder for water flow and hydration. During the oven-drying process, the release of water is facilitated by being more superficially present in the open pores, not significantly interfering with internal defects. This is indicative

of greater durability and rigidity of this lot (5W 950°C) relative to the others.

Fig. 11 presents the Weibull diagram, showing the failure probability analysis of the ceramics studied at the sintering temperature of 950°C. The linear regression of the experimental data allowed us to obtain the Weibull  $m$  parameter [Fig. 11(a)] and the characteristic stress. The results of the characteristic stress that define the scaling factor of the intact samples are as follows: 4.3 MPa for the 0W samples, 4.3 MPa for the 5W sample, and 4.2 MPa for the 10W samples. These values represent the position below which the material will not fail.

#### Weibull Diagram of Intact Samples

The values of the coefficient of determination,  $r^2$ , suggest less scattering of the data in the 5W samples, and the value of the characteristic stress relative to the value below which the material does not fail is equal for the 0W samples. The lower scattering of the data is reflected in the larger  $m$  parameter ( $m = 11.4$ ), that is, this set of samples is more homogeneous, has a lower probability of failure, and therefore is more reliable. These results converge in Fig. 10. The results obtained for modulus ( $m$ ) are within the range expected

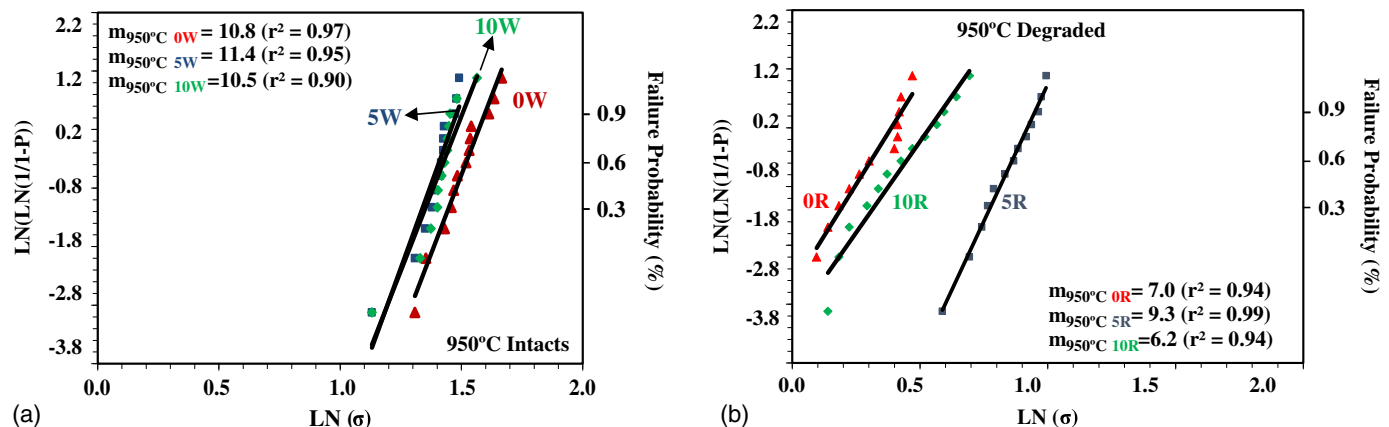


**Fig. 11.** Weibull diagram for red ceramic sintered at (a) 950°C intact; and (b) degraded.

for ceramic materials (Zanotto and Migliori 1991; Pinheiro and Holanda 2010).

The 10W samples presented an  $r^2$  of 0.90, that is, higher data dispersion, reflecting the lower value of the Weibull parameter ( $m = 10.5$ ).

The results of the characteristic stress of the degraded samples are as follows: 1.5 MPa for 0W samples, 2.5 MPa for 5W samples, and 1.6 MPa for 10W samples. These results show that the wetting-drying cycles cause an increase in the probability of failure, that is, the faults can begin to occur at smaller strength values.

### Weibull Diagram of Samples after 200 Cycles

Fig. 11(b) also shows that the Weibull parameter was reduced for all cases; however, the 5W samples presented the highest value ( $m = 9.3$ ) and the best fit ( $r^2 = 0.99$ ), making it the more reliable sample set, corroborated in Fig. 10.

All the results show unimodal performance, that is, the samples present the same set of defects represented by the open pores (Zanotto and Migliore 1991; Pinheiro and Holanda 2010), as shown in Fig. 8, referring to the increase of the water absorption (Fig. 7) of intact and degraded samples (200 cycles), except 5W 950°C, because they are statistically the same since the deviations are coincident.

### Stress-Strain Curves of Intact Samples

Fig. 12 shows the stress-strain curves for the 0W and 5W samples sintered at 950°C, both intact and after 200 wetting-drying cycles.

Fig. 12 shows that the stress-strain behavior of the intact materials is similar, given that up to 1% strain the behavior is linear with very close flexural stress levels ( $FS$ ) for intact samples 0W and 5W. Higher values of flexural stress were observed in the intact 5W samples for all strains ( $\varepsilon$ ), reflecting greater rigidity ( $E = 1.2 \pm 0.05$  GPa), as was also seen in Figs. 10 and 11 when compared with intact 0W samples ( $E = 1.0 \pm 0.04$  GPa). These values are in agreement with Pinheiro and Holanda (2010). Above 1% strain, all samples exhibit nonlinear behavior until they reach the resistance peak strength and rupture.

### Stress-Strain Curves of Samples after 200 Cycles

The elastic modulus before ( $E = 1.0 \pm 0.08$  GPa) and after ( $E = 0.7 \pm 0.09$  GPa) the wetting-drying cycles declined by 30% in the 0W samples (Figs. 10 and 11). These samples deform more than the

5W samples at lower levels of strength, that is, they have lower rigidity, and consequently more weakening. This is attributable to the low amount of alkali (Table 5) in the composition of the clay, resulting in a less vitreous phase after sintering, leading to rupture in the pores due to the concentration of tension at these fragile points.

The wetting-drying cycles had a greater influence on the loss of strength (59.5% for 0W and 42.2% for 5W) than on the reduction of rigidity ( $E$ ). This is due to the greater strain of the 0W samples, as measured by the displacement of the deflection in the three-point bending test (Fig. 10).

The 5W samples have fewer pores (Fig. 8) and higher strength (Fig. 10) and rigidity before and after degradation. This indicates a tendency for longer durability, as well as greater reliability and a lower probability of failure (Fig. 11). This favors the incorporation of ornamental stone waste material into clay mixtures for the manufacture of red ceramic structural blocks because it improves the overall performance of the construction.

### Useful Life of Samples

The results of Figs. 7–10 indicate lower degradation was for the 5W samples before and after degradation. Therefore, the effect of reduction of the property of interest after 200 cycles in the samples was highest for the flexural strength (Fig. 10), by the magnitude of loss to be the largest of them. Based on this observation, the long-term useful life can be determined by comparing the laboratory degradation time, 200 cycles, with the local weathering degradation time of 5 years for the same loss of flexural strength index. The correlation was done with the 0W samples sintered at 950°C.

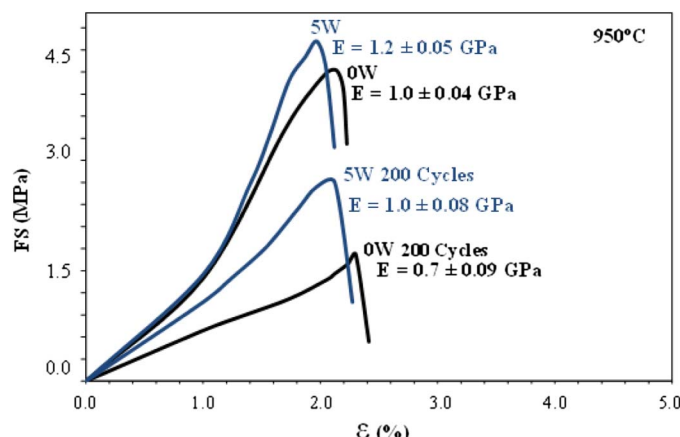
Fig. 13 shows the loss of flexural strength index for 0W and 5W samples of red ceramic parts sintered at 950°C (a) and the long-term forecast (b), in defining the useful life of the material investigated.

Fig. 13(a) shows the nonlinear trend of the loss of flexural strength index over almost the entire degradation time, independent of the degradation process, in addition to a tendency to stabilize at the end of degradation. The final values of mechanical weakening were 59.5% and 42.4% for 0W and 5W, respectively, after 200 cycles, and 57% and 38.5% for 0W and 5W after 5 years (1,825 days) of local weathering. The 5W samples showed less weakening, independent of the degradation process, that is, the performance was better.

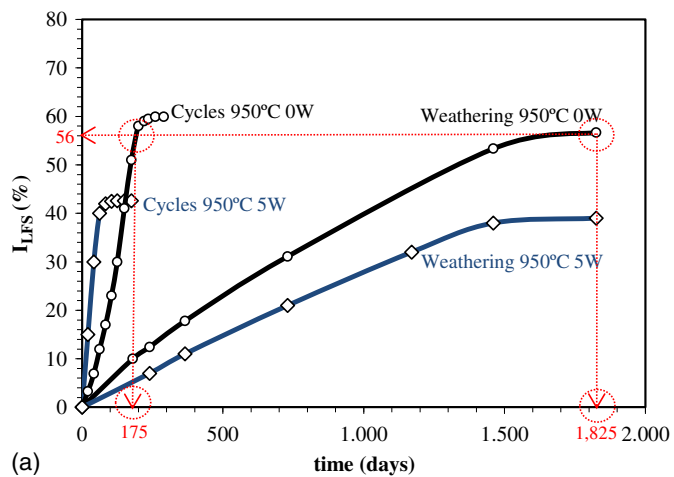
When comparing the process of laboratory degradation with that of exposure to the local environment, the percentage values of weakening are close, indicating that the laboratory procedure is similar to what occurs in the external constructed environment. That is, the laboratory procedure represents the mechanisms of degradation, such as solar radiation, temperature variation, relative air humidity, rainfall, and wind incidence, despite being more aggressive. The biggest difference is in the time periods of 200 days for the cycles and 1,825 days for weathering.

In Fig. 13(b), the 0W results show a region of departure from the curve model from 150 cycles; however, the  $r^2$  of the equation is 0.99, meaning that 1% of the data are outside of the model, allowing extrapolation with some accuracy. All of the statistical treatments presented in this study have an accuracy of 5%, that is, it allows 5% of the observed data to be more distant from the mean, and therefore, to be rejected.

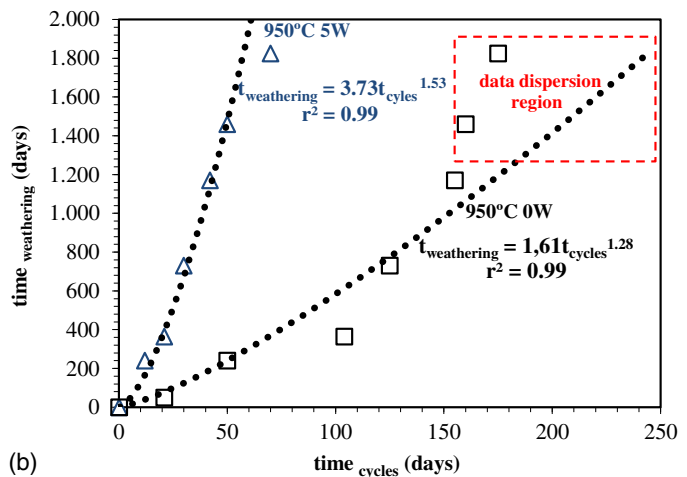
The useful life of the red ceramic samples was calculated from the equations in Fig. 13(b) obtained by correlating the laboratory degradation time with the weathering time, so that the samples weakened to 1.5 MPa; in this case, the value considered was  $t_{cycles} = 300$ . For the 0W samples of Fig. 13(b), the result was 4.8 years, and for the 5W samples the result was 14 years.



**Fig. 12.** Stress-strain behavior for red ceramic sintered at 950°C intact and degraded.



(a)



(b)

**Fig. 13.** Curves of (a) loss of flexural strength index; and (b) useful life of the red ceramic 0W and 5W samples sintered at 950°C.

Hence, the incorporation of 5% of ornamental stone waste material increases the useful life of red ceramic products 2.91-fold under local weather conditions. This conclusion is made for red ceramic bricks and blocks without mechanical protection (i.e., plaster), a common practice in the Campos-RJ region, especially in walls more than 3 m high in luxury condominiums.

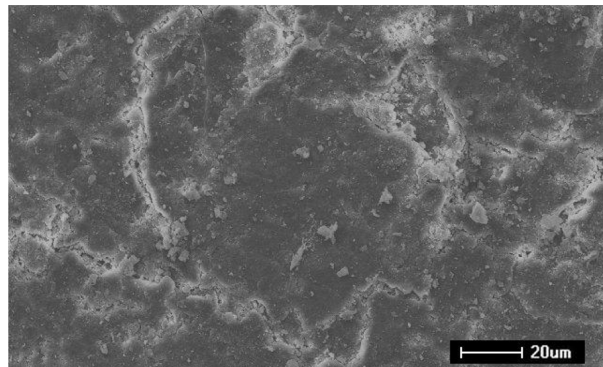
This demonstrates the importance of the incorporation of ornamental stone waste in red ceramics, improving the final product and increasing the rigidity and durability of the part, thereby also improving quality assurance and deadline compliance. Moreover,

the incorporation of stone waste in red ceramics makes it inert, contributing to the proper disposition of the waste.

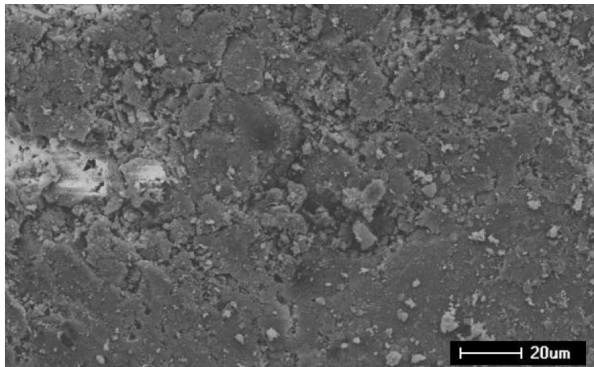
Fig. 14 shows the micrographs of the evolution of degradation after 200 wetting-drying cycles in comparison with the intact samples obtained by scanning electron microscopy.

#### SEM Micrographs of the Intact Samples

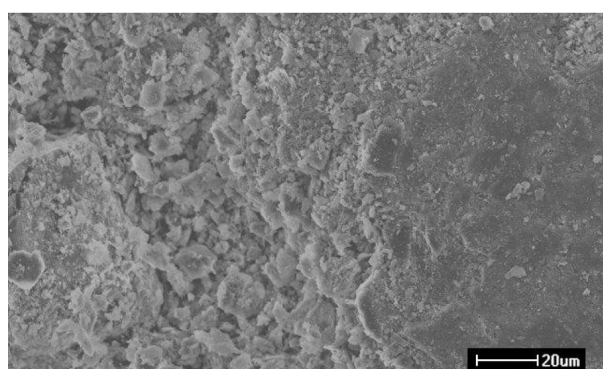
Figs. 14(a and b) show the surface micrograph of 0W samples sintered at 950°C before and after 200 wetting-drying cycles.



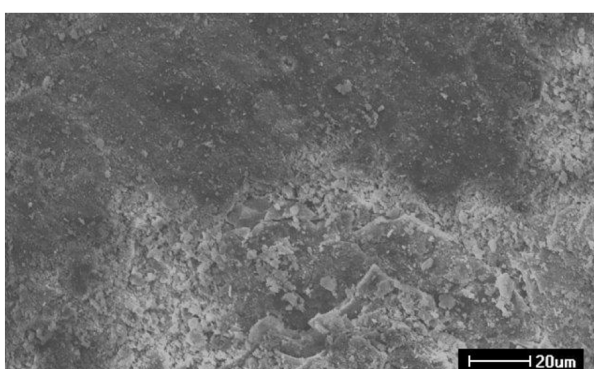
(a)



(b)



(c)



(d)

**Fig. 14.** SEM micrographs of red ceramic: (a) 0W 950°C intact; (b) 5W 950°C intact; (c) 0W 950°C after 200 cycles; and (d) 5W 950°C after 200 cycles.

The surface shown in Fig. 14(a) is less rough and porous than the 5W sample at 950°C [Fig. 14(b)]; however, it is quite fissured, which leads to lower flexural strength (Fig. 10), lower Weibull modulus (Fig. 11), and higher strain at lower stress levels (Fig. 12). Fig. 14(b) shows more loose particles and surface porosity than the sample shown in Fig. 14(a).

### SEM Micrographs of the Samples after 200 Cycles

Fig. 14(c) shows a scattering of surface particles, greater depth of degradation, and greater porosity when compared with Fig. 14(d). Fig. 14(d) shows lower surface porosity and a few loose particles. When compared with Fig. 14(b), the surface wear due to cycles makes the surface smoother than the surface shown in Fig. 14(a), which leaches out the surface mass, showing that the surface pores of the 5W sample had no interconnectivity with the interior of the part, and therefore water absorption and apparent porosity were lower [Figs. 7(b) and 8(b)].

Fig. 14(d) also shows that the surface of the 5W sample sintered at 950°C is less rough than that shown in Fig. 14(a). This is due to better packing in samples with the incorporation of stone waste, favored by the presence of  $K_2O + Na_2O + CaO$  represented by muscovite + biotite + calcite = 17.6% (Fig. 4 and Table 4), than in those without waste material (Fig. 3). This shows that the Weibull modulus is directly related to the defects in the part, leading to a lower strain (Fig. 12) and an almost three times longer life (Fig. 13).

## Conclusions

The results of this study show that the incorporation of ornamental stone waste, at levels of 5% by mass, into the production of red ceramic parts, can increase the flexural strength 2.91-fold (to 14 years) and the durability of the material when compared with the red ceramic parts without the stone waste (to 4.8 years). This is due to the presence of alkali and earth alkali in the ornamental stone residue that form molten flux during sintering and a vitreous phase during cooling, providing lower apparent porosity, higher statistical homogeneity, less deformability, longer durability, and lower surface roughness (SEM micrographs). The durability was demonstrated in terms of future time, which is an advance, since evaluation of durability has typically been qualitative, by comparison of one material with another, without defining the relative increase in service life. The residue material used is nonhazardous and non-toxic and the incorporation into the clay makes the residue inert. In the case of disposal of this material, due to defects or after demolition, it is not considered hazardous. The wetting–drying cycles were used to represent the majority of the environmental degradation mechanisms, especially those present in tropical countries like Brazil, but this procedure is applicable in any climate.

## References

- ABNT (Brazilian Association of Technical Standards). 1984. *Determination of the granulometric analysis of soils*. [In Portuguese.] NBR 7181. Rio de Janeiro, Brazil: ABNT.
- ABNT (Brazilian Association of Technical Standards). 2004a. *Procedure for obtention leaching extract of solid wastes*. [In Portuguese.] NBR 10005. Rio de Janeiro, Brazil: ABNT.
- ABNT (Brazilian Association of Technical Standards). 2004b. *Procedure for obtention of solubilized extraction of solid wastes*. [In Portuguese.] NBR 10006. Rio de Janeiro, Brazil: ABNT.
- ABNT (Brazilian Association of Technical Standards). 2004c. *Solids waste—Classification*. [In Portuguese.] NBR 10004. Rio de Janeiro, Brazil: ABNT.
- ABNT (Brazilian Association of Technical Standards). 2005. *Ceramic components. Part 1: Hollow ceramic blocks for non-load-bearing masonry, terminology and requirements*. [In Portuguese.] NBR 15270-1. Rio de Janeiro, Brazil: ABNT.
- ABNT (Brazilian Association of Technical Standards). 2009. *Ceramic components—Ceramic roof tiles—Terminology, requirements and testing methods*. [In Portuguese.] NBR 15310. Rio de Janeiro, Brazil: ABNT.
- Acchar, W., F. A. Vieira, and D. Hotza. 2006a. “Effect of marble and granite sludge in clay materials.” *Mater. Sci. Eng. A*, 435–436 (1): 606–610. <https://doi.org/10.1016/j.msea.2006.07.091>.
- Acchar, W., F. V. Vieira, and A. M. Segadães. 2006b. “Using ornamental stone cutting rejects as raw materials for red clay ceramic products: Properties and microstructure development.” *Mater. Sci. Eng. A*, 419 (1–2): 306–309. <https://doi.org/10.1016/j.msea.2006.01.021>.
- Alexandre, J., A. R. G. Azevedo, G. C. Xavier, F. M. Muylaert, S. N. Monteiro, F. B. Oliveira, N. G. Azeredo, and C. P. Bozzi. 2016. “Influence of weather exposure on dimensional changes in clay ceramics incorporated with granite waste.” *Mater. Sci. Forum*, 869 (1): 131–135. <https://doi.org/10.4028/www.scientific.net/MSF.869.131>.
- ASTM. 1972. *Standard test method for water absorption, bulk density, apparent porosity, and apparent specific gravity of fired whiteware products*. ASTM C373. West Conshohocken, PA: ASTM.
- ASTM. 1977. *Flexural properties of ceramic whiteware materials*. ASTM C674. West Conshohocken, PA: ASTM.
- Barba, A., V. Beltrán, C. Feliu, J. García, F. Ginés, E. Sánchez, and V. Sans. 2002. *Materias Primas para la Fabricación de Soportes de Baldosas Cerámicas*. 2nd ed. Castellón de la Plana, Spain: Instituto de Tecnología Cerámica.
- Brooks, R. M., and M. Cetin. 2013. “Water susceptible properties of silt loam soil in sub grades in south west Pennsylvania.” *Int. J. Modern Eng. Res.*, 3 (2): 599–603.
- Celik, H. 2010. “Technological characterization and industrial application of two Turkish clays for the ceramic industry.” *Appl. Clay Sci.*, 50 (2): 245–254. <https://doi.org/10.1016/j.clay.2010.08.005>.
- Emiliani, G. P., and F. Corbara. 1999. *Tecnología Cerámica-La Lavorazione*, 97–99. Faenza, Italy: Gruppo Editorial e Faenza Editrice.
- Gomes, R. F., G. C. Xavier, F. A. J. Saboya, P. C. A. Maia, J. Alexandre, and L. G. Pedrotti. 2014. “Degradation of red ceramic with incorporated of petroleum waste.” *Mater. Sci. Forum*, 798–799 (1): 257–262. <https://doi.org/10.4028/www.scientific.net/MSF.798-799.257>.
- INMET (National Institute of Meteorology). 2016. “Meteorological database for teaching and research.” Accessed August 2, 2018. <http://www.inmet.gov.br/portal/index.php?r=bdmep/bdmep>.
- Krakowiak, K. J., P. B. Lourenço, and F. J. Ulm. 2011. “Multitechnique investigation of extruded clay brick microstructure.” *J. Am. Ceram. Soc.*, 94 (9): 3012–3022. <https://doi.org/10.1111/j.1551-2916.2011.04484.x>.
- Manhães, J. P. V. T., and J. N. F. Holanda. 2008. “Characterization and classification of granitic rock powder solid waste produced by ornamental rock industry.” *Química Nova (Rio)*, 31 (6): 1301–1304.
- Monteiro, S. N., and C. M. F. Vieira. 2014. “On the production of fired clay bricks from waste materials: A critical update.” *Constr. Build. Mater.*, 68 (1): 599–610. <https://doi.org/10.1016/j.conbuildmat.2014.07.006>.
- Munz, D., and T. Fett. 1999. Vol. 36 of *Ceramics*, 1st ed. Berlin: Springer.
- Murthy, D. N. P., M. Xie, and R. Jiang. 2004. *Weibull models*. Hoboken, NJ: Wiley.
- Mymrin, V. A., K. P. Alekseev, E. V. Zelinskaya, N. A. Tolmacheva, and R. E. Catai. 2014. “Industrial sewage slurry utilization for red ceramics production.” *Constr. Build. Mater.*, 66 (1): 368–374. <https://doi.org/10.1016/j.conbuildmat.2014.05.036>.
- Mynrim, V., K. Alekseev, O. M. Fortini, and R. E. Catai. 2017. “Water cleaning sludge as principal component of composites to enhance mechanical properties of ecologically clean red ceramics.” *J. Cleaner Prod.*, 145 (1): 367–373. <https://doi.org/10.1016/j.jclepro.2016.12.141>.
- Nandi, V. S., F. Raupp-Pereira, O. R. K. Montedo, and A. P. N. Oliveira. 2015. “The use of ceramic sludge and recycled glass to obtain engobes

- for manufacturing ceramic tiles.” *J. Cleaner Prod.* 86 (1): 461–470. <https://doi.org/10.1016/j.jclepro.2014.08.091>.
- Okunade, E. A. 2008. “The effect of wood ash and sawdust admixtures on the engineering properties of a burnt laterite-clay brick.” *J. Appl. Sci.* 8 (6): 1042–1048. <https://doi.org/10.3923/jas.2008.1042.1048>.
- Pérez-Villarejo, L., F. A. Corpas-Iglesias, S. Martínez-Martínez, R. Artiaga, and J. Pascual-Cosp. 2012. “Manufacturing new ceramic materials from clay and red mud derived from the aluminium industry.” *Constr. Build. Mater.* 35 (1): 656–665. <https://doi.org/10.1016/j.conbuildmat.2012.04.133>.
- Pinheiro, B. C. A., and J. N. F. Holanda. 2010. “Effect of the firing temperature on some mechanical properties of red ceramic.” *Cerâmica* 56 (1): 237–243. <https://doi.org/10.1590/S0366-69132010000300005>.
- Ribeiro, D. V., S. C. Figueiredo, A. T. Machado, F. R. V. Diaz, and C. A. C. Souza. 2015. “Evaluation of the incorporation of waste generated from titanium dioxide manufacturing in red ceramics.” *Mater. Res.* 18 (1): 98–105. <https://doi.org/10.1590/1516-1439.274414>.
- Rodrigues, D. V., G. C. Xavier, F. Saboya, P. C. A. Maia, and J. Alexandre. 2012. “Durability of red ceramic samples with addition of ornamental rock waste free of steel particles.” *Cerâmica* 58 (1): 286–293.
- Rozenstrauba, I., D. Bajare, R. Cimdins, L. Berzina, J. Bossert, and A. R. Boccaccini. 2006. “The influence of various additions on a glass-ceramic matrix composition based on industrial waste.” *Ceram. Int.* 32 (2): 115–119. <https://doi.org/10.1016/j.ceramint.2005.01.006>.
- Saboya, F., G. C. Xavier, and J. Alexandre. 2007. “The use of the powder marble by-product to enhance the properties of brick ceramic.” *Constr. Build. Mater.* 21 (10): 1950–1960. <https://doi.org/10.1016/j.conbuildmat.2006.05.029>.
- Santos, P., C. Martins, and E. Júlio. 2015. “Enhancement of the thermal performance of perforated clay brick walls through the addition of industrial nano-crystalline aluminium sludge.” *Constr. Build. Mater.* 101 (1): 227–238. <https://doi.org/10.1016/j.conbuildmat.2015.10.058>.
- Santos, P. S. 1989. *Science and technology of clays*. [In Portuguese.] 2nd ed. São Paulo, Brazil: Edgard Blücher.
- Somiya, S. 1990. *Handbook of advanced ceramics*, 1046–1058. New York: Elsevier.
- Stryszewska, T. 2014. “The change in selected properties of ceramic materials obtained from ceramic brick treated by the sulphate and chloride ions.” *Constr. Build. Mater.* 66 (1): 268–274. <https://doi.org/10.1016/j.conbuildmat.2014.05.066>.
- Torres, P., H. R. Fernandes, S. Olhero, and J. M. F. Ferreira. 2009. “Incorporation of wastes from granite rock cutting and polishing industries to produce roof tiles.” *J. Eur. Ceram. Soc.* 29 (1): 23–30. <https://doi.org/10.1016/j.jeurceramsoc.2008.05.045>.
- Vieira, C. M. F., and J. V. Emiliano. 2013. “Incorporation of sedimentary powder rock in roofing tiles body. Part 1: Effect in the physical and mechanical properties.” [in Portuguese.] *Cerâmica* 59 (1): 2349–2356. <https://doi.org/10.1590/S0366-691320130000300007>.
- Vieira, C. M. F., B. Silva, and J. P. R. G. Carvalho. 2016. “Recycling of granite waste from sawing operation in clay brick for civil construction.” *Modern Environ. Sci. Eng.* 2 (6): 389–395. [https://doi.org/10.15341/mese\(2333-2581\)06.02.2016/004](https://doi.org/10.15341/mese(2333-2581)06.02.2016/004).
- Vieira, C. M. F., T. M. Soares, R. Sánchez, and S. N. Monteiro. 2004. “Incorporation of granite waste in red ceramics.” *Mater. Sci. Eng. A* 373 (1–2): 115–121. <https://doi.org/10.1016/j.msea.2003.12.038>.
- Vitorino, J. P. D., S. N. Monteiro, and C. M. F. Vieira. 2009. “Characterization and incorporation of wastes from water treatment plant into clayey ceramic.” *Cerâmica* 55 (336): 385–392. <https://doi.org/10.1590/S0366-69132009000400008>.
- Wiemes, L., U. Pawlowsky, and V. Myrrin. 2017. “Incorporation of industrial wastes as raw materials in brick’s formulation.” *J. Cleaner Prod.* 142 (1): 69–77. <https://doi.org/10.1016/j.jclepro.2016.06.174>.
- Xavier, G. C., F. A. J. Saboya, P. C. A. Maia, and J. Alexandre. 2012. “Durability of fired clay bricks containing granite powder.” *Materiales de Construcción* 62 (306): 213–229. <https://doi.org/10.3989/mc.2012.60710>.
- Xavier, G. C., F. A. J. Saboya, P. C. A. Maia, J. Alexandre, and L. G. Pedroti. 2014. “Red ceramic with addition of petroleum coke.” *Mater. Sci. Forum* 798–799 (1): 263–268. <https://doi.org/10.4028/www.scientific.net/MSF.798-799.263>.
- Zanotto, E. D., and A. R. Migliori Jr. 1991. “Mechanical properties of ceramic materials: An introduction.” *Cerâmica* 37 (1): 7–16.